Rapid Communications

Effect of Zeeman coupling on the Majorana vortex modes in iron-based topological superconductors

Areg Ghazaryan, P. L. S. Lopes, Pavan Hosur, Matthew J. Gilbert, 4,5,6 and Pouyan Ghaemi^{7,8} ¹IST Austria (Institute of Science and Technology Austria), Am Campus 1, 3400 Klosterneuburg, Austria ²Stewart Blusson Quantum Matter Institute, University of British Columbia, Vancouver, British Columbia, Canada V6T 1Z4 ³Department of Physics, University of Houston, Houston, Texas 77204, USA ⁴Micro and Nanotechnology Laboratory, University of Illinois at Urbana-Champaign, Urbana, Illinois 61801, USA ⁵Department of Electrical and Computer Engineering, University of Illinois at Urbana-Champaign, Urbana, Illinois 61801, USA ⁶Department of Electrical Engineering, Stanford University, Stanford, California 94305, USA ⁷Physics Department, City College of the City University of New York, New York, New York 10031, USA ⁸Physics Program, Graduate Center of the City University of New York, New York 10031, USA



(Received 24 July 2019; revised manuscript received 14 December 2019; published 13 January 2020)

In the superconducting regime of $\text{FeTe}_{(1-x)}\text{Se}_x$, there exist two types of vortices which are distinguished by the presence or absence of zero-energy states in their core. To understand their origin, we examine the interplay of Zeeman coupling and superconducting pairings in three-dimensional metals with band inversion. Weak Zeeman fields are found to suppress intraorbital spin-singlet pairing, known to localize the states at the ends of the vortices on the surface. On the other hand, an orbital-triplet pairing is shown to be stable against Zeeman interactions, but leads to delocalized zero-energy Majorana modes which extend through the vortex. In contrast, the finite-energy vortex modes remain localized at the vortex ends even when the pairing is of orbital-triplet form. Phenomenologically, this manifests as an observed disappearance of zero-bias peaks within the cores of topological vortices upon an increase of the applied magnetic field. The presence of magnetic impurities in $FeTe_{(1-x)}Se_x$, which are attracted to the vortices, would lead to such Zeeman-induced delocalization of Majorana modes in a fraction of vortices that capture a large enough number of magnetic impurities. Our results provide an explanation for the dichotomy between topological and nontopological vortices recently observed in $FeTe_{(1-x)}Se_x$.

DOI: 10.1103/PhysRevB.101.020504

Introduction. To date, one of the major impediments in the search for Majorana fermions (MFs) is the required intrinsic [1,2] or induced [3–6] topological superconductivity. Of the available materials that possess topology, superconductivity, and magnetism, iron-based superconductors are of recent interest [7–15]. In particular, FeTe_{0.55}Se_{0.45} (FTS) has recently been shown to have band inversion that results in a helical, topologically protected, Dirac cone on the surface [16–19]. The phenomenology of vortices, proliferated in the presence of magnetic fields, is also noteworthy in FTS [20-23]. The low charge density in FTS is experimentally advantageous as it results in large Caroli–de Gennes–Matricon (CDM) vortexmode gaps [24] which facilitate the spectral detection of zero-energy vortex modes via scanning tunneling microscopy (STM).

While evidence of MFs in FTS has been observed, a comprehensive understanding of the salient physics of the vortex composition is lacking. More precisely, the energy spectra of the vortices follow two different hierarchies relative to the CDM vortex gap, $\delta = \frac{\Delta^2}{\mu}$, where Δ is the bulk superconducting gap and μ is the chemical potential. The trivial vortex energy spectrum scales as $(n + 1/2)\delta$ (with $n \in \mathbb{Z}$), which does not include the zero mode, whereas the topological vortices follow $n\delta$. Additionally, the percentage of vortices with zeroenergy modes decreases as the perpendicular magnetic field increases, even though the intervortex distances are larger than the superconducting coherence length [20,21,25,26]. Moreover, the distribution of vortices with and without a zero mode has no correlation with the charge disorder on the surface of the material [21]. These features, on aggregate, suggest that the properties that distinguish the two classes of vortices stem from the bulk properties of the individual vortex rather than those of the surface states. In particular, the effects of magnetic field, beyond the generation of vortices, might crucially affect the properties of the superconducting state and the vortices.

Motivated by experimental observations, we examine the effects of Zeeman coupling on the vortex modes in FTS. As the topological properties of FTS are driven by band inversion, we eschew more complex band models and utilize a simple model of a doped three-dimensional (3D) time-reversal symmetric (TRS) topological insulator (TI) which has been used as an appropriate toy model to investigate the properties of vortices in FTS [27–29]. Due to the strong spin-orbit coupling, the Zeeman field splits the degenerate Fermi surface in TRS TIs into two helical Fermi surfaces with opposite helicity [30]. In this Rapid Communication, we show that the split Fermi surfaces prefer an orbital-triplet superconducting pairing which delocalizes the MF modes at the ends of the vortices on the surface. To make a direct connection with the

dichotomy of vortices in FTS we note that the Zeeman field would result from the magnetic impurities along the vortex core [31,32]. Interestingly, such magnetic Fe impurities are known to exist in FTS [33,34] and interact with the vortices [31]. In addition, an increase of magnetic field naturally leads to the enhancement of Zeeman coupling, which further destabilizes the topological vortices, as is experimentally observed. We should also note that neutron scattering measurements have shown evidence of ferromagnetic clusters of Fe atoms in FTS [33]. Therefore, the decrease of the concentration of Fe impurities is directly linked to an increase of the fraction of topological vortices. The observation of clusters of vortices, with and without zero-energy vortex modes, would further support our theory.

Model Hamiltonian. The 3D TRS TI is represented by the tight-binding Hamiltonian $\mathcal{H}_{\mathbf{k}} = \sum_{\mathbf{k}} \psi_{\mathbf{k}}^{\dagger} [\tau_{x} \mathbf{d}_{\mathbf{k}}.\sigma + m_{\mathbf{k}}\tau_{z} - \mu] \psi_{\mathbf{k}}$, where Pauli matrices σ_{i} and τ_{i} act on spin and orbital space, respectively, $d_{k_{i}} = 2t \sin(k_{i})$, $m_{\mathbf{k}} = M + m_{0} \sum_{i} \cos(k_{i})$, and M, m_{0} , t are parameters of the model, and μ is the chemical potential. By varying the parameters, this model Hamiltonian represents both strong and weak TRS TIs [35]. The tight-binding model is used for the numerical calculations while our analytical results are based on the effective model,

$$\mathcal{H} = \hbar v_F \tau_x \boldsymbol{\sigma} \cdot \mathbf{k} + m_k \tau_z, \tag{1}$$

where $m_k = m + \epsilon k^2$ is the effective mass term and **k** is the momentum relative to the center of the Brillouin zone. The trivial (topological) insulator corresponds to $m\epsilon > 0$ (< 0). Without loss of generality, we take $\hbar v_F = 1$.

With the Hamiltonian defined, we begin our analysis in the metallic phase, when $\mu > |m|$. The model displays two degenerate Fermi surfaces that split by a Zeeman field Δ_Z . Since the bulk band structure gap is large compared with superconducting gap, we use the effective Hamiltonian resulting from projecting the Hamiltonian in Eq. (1) into the states at the two Fermi surfaces,

$$\mathcal{H} = \int d^3 \mathbf{k} f_{\mathbf{k}}^{\dagger} [(E_{\mathbf{k}} - \mu) \nu_0 + \mathbf{d}_{\mathbf{k}} \cdot \mathbf{v}] f_{\mathbf{k}}. \tag{2}$$

Here, ν_i 's are the identity or Pauli matrices acting on the space of two Fermi surfaces. The vector $\mathbf{d_k} = \frac{\Delta_Z}{2}(-\frac{m_k}{E_k}\frac{k_x^2 + k_y^2}{|\mathbf{k}|}, 0, \frac{k_z}{k})$ represents the Zeeman field and f_k is the fermion fields ψ_k projected onto the Fermi surfaces [30]. The two Fermi spin-split Fermi surfaces are identified by diagonalizing the projected Hamitonian (2) in the ν space.

A previous analysis [36] identified two types of superconductivity in doped TIs which are energetically favorable: an intraorbital spin singlet, $\int d^3 \mathbf{r} \psi^\dagger \Delta i \tau_0 \sigma_y \psi^{\dagger T} + \text{H.c.}$, and an interorbital orbital-triplet spin singlet, $\int d^2 \mathbf{k} \psi_{\mathbf{k}}^\dagger i \tau_x \sigma_y \psi_{-\mathbf{k}}^{\dagger T} + \text{H.c.}$ Henceforth, we will refer to these superconducting pairings as intraorbital-singlet and interorbital-triplet pairings, respectively.

Upon projection onto the Fermi surfaces, the superconducting pairing potentials assume the following form,

$$\frac{\Delta_{\alpha}}{2} \int d^3 \mathbf{k} f_{\mathbf{k}}^{\dagger} e^{-i\phi_{\mathbf{k}}} \nu_{\alpha} f_{-\mathbf{k}}^{\dagger T}, \tag{3}$$

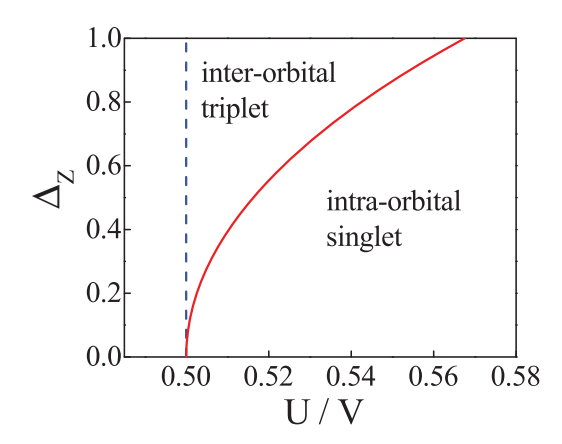


FIG. 1. Phase boundaries between regions with superconducting order parameters Δ_1 or Δ_0 as a function of the ratio U/V of interaction strengths of each channel and the field magnitude Δ_Z (red solid curve). The blue dashed line is a guide for the eye of the case when $\Delta_Z=0$. The parameters of the Hamiltonian are m=-0.5 and $\epsilon=0.5$. Increased Zeeman coupling results in larger regions where interorbital-triplet pairing is the ground state.

where for the intraorbital-singlet pairing $\alpha=1$ and for interorbital-triplet pairing $\alpha=0$. Examination of the superconducting pairing term in Eq. (3) in comparison with the kinetic Hamiltonian in Eq. (2) shows that the intraorbital-singlet pairing Δ_1 corresponds to pairing electrons between different Zeeman split Fermi surfaces. In contrast, the interorbital-triplet pairing Δ_0 pairs electrons solely within each of the Zeeman split Fermi surfaces. Thus, the effect of Zeeman coupling is to break the TRS within the model and unbalance the two pairing potentials in favor of Δ_0 which couples the electrons solely within each Zeeman split Fermi surface [37].

To examine the outlined effect of Zeeman coupling on the dominant form of superconducting pairing, we utilize a linear gap equation [30] to determine the critical temperatures of the two superconducting pairings [36,38–40]. The corresponding U-V model, in which U and V are the intra- and interorbital interactions, leads to the equation

$$\det \begin{vmatrix} U\bar{\chi} - 1 & U\chi_2 \\ V\chi_2 & V\chi_1 - 1 \end{vmatrix} = 1, \quad V\chi_0 = 1.$$
 (4)

Here, $\bar{\chi}$, χ_1 , and χ_2 are the superconducting susceptibilities characterizing intraorbital spin-singlet pairing and χ_0 describes the interorbital spin-triplet pairing. $\bar{\chi} = -\int_{-w_D}^{w_D} \mathcal{D}(\xi) \tanh{(\xi/2T)/2\xi}d\xi$ is the standard s-wave susceptibility, $D(\xi)$ is the density of states, and w_D is the Debye frequency.

By numerically solving the U-V Eq. (4), we obtain the critical temperature T_c for each pairing channel. Figure 1 shows the resulting phase boundaries that delineate the regions where either Δ_0 or Δ_1 correspond to a higher critical temperature and so is the dominant form of pairing. In Fig. 1, we plot the phase boundary as we vary Δ_Z and the ratio U/V. It is evident in Fig. 1 that the inclusion of the Zeeman effect results in an enhancement of the triplet (Δ_0) pairing and the suppression of the singlet one (Δ_1) at a given chemical potential.

Vortex modes. Having established the phase diagram of the superconducting pairing, we proceed to study the internal structure of the vortices as we insert a π -flux tube into the pairing potential: $\Delta_{\alpha}(r) = |\Delta_{\alpha}(r)|e^{i\theta}$ [41,42]. Since the coherence length FTS is in the range of 2–10 nm [19,20,25] and the observed distance between vortices is around 30 nm for magnetic fields up to 6 T [21,22], we disregard intervortex hybridization effects and concentrate on the physical properties of a single vortex. We fix $k_z = 0$ as we are interested in points where the topological \mathbb{Z}_2 index changes and this only occurs at $k_z = 0$ or π . Since the vortex modes stem from states close to the Fermi energy, their wave functions can be expressed in terms of a superposition of the TI conduction band eigenstates in the cylindrical coordinates $\chi_{l,k}^{\nu}$ [30]. Here, l's are angular momentum quantum numbers and $\nu = \pm$ correspond to the two energy bands of Hamiltonian (1) which are split by Zeeman coupling.

Given the rotational symmetry of the vortex profile, the vortex modes with different l's do not hybridize and the vortex Hamiltonian decouples into sectors with fixed l. Also, for interorbital-triplet pairing, the vortex does not mix the ν 's. On the other hand [30], the translation symmetry in the plane perpendicular to the vortex is broken and different radial momenta k, as well as Nambu particle-hole states, are mixed by the vortex. The effective vortex Hamiltonian acting in the radial momentum and Nambu particle-hole spaces take the form of a 1D Jackiw-Rebbi model [43],

$$H_{l}^{\nu} = \Pi_{z} \frac{\Delta_{0} \lambda_{\nu}(k)}{\xi_{0}} + \Pi_{y} \frac{\Delta_{0}}{\xi_{0}} (i\partial_{k}) + \Pi_{x} E_{l,0}^{\nu}(k).$$
 (5)

The Π matrices act on a Nambu space, ξ_0 is the superconducting coherence length, and $\Delta_0 \lambda_{\nu}(k)/\xi_0 = k + \frac{hm_k}{2E_0^0} \nu$ μ. The Jackiw-Rebbi lowest-energy solutions are localized at the Fermi surface where the coefficient $\lambda_{\nu}(k_F^{\nu})$ changes sign. These states have the form $e^{-\int_{k_F^{\prime}-k}^{k_F^{\prime}+k} dk' \lambda_v(k')} (1,1)^T$ in the Nambu particle-hole basis and have energy $E_{l,0}^{\nu}(k_F)$. Notice that vortex-mode wave functions are exponentially localized around the Fermi wave vector. Since the Bogoliubov-de Gennes (BdG) Hamiltonian in Eq. (5) is in the basis of the TI conduction band states, the full wave function of the two vortex modes (each associated with one Zeeman split Fermi surface) takes the form $\Psi_V^{\nu}(l,r) \approx \chi_{l,k_F}^{\nu}(r)(1,1)_{\Pi}^T$, where $(1,1)_{\Pi}^{T}$ is the spinor in Nambu particle-hole space. Previously, a similar result was obtained for the intraorbital spin-singlet case [41,42]. In that case, solutions were again centered at the metallic phase Fermi surface, with corresponding energies $E_{l,1}^{\nu} = \frac{\Delta}{k_F \xi_1} (2\pi l + \pi + \nu \phi_B)$. ϕ_B is a Berry-phase-like term which permits zero modes whenever $\phi_B = \pi$. In contrast, for the interorbital-triplet case, the energies of the vortex modes are $E_{l,0}^{\nu} = \frac{\Delta_0}{k_F^{\nu} \xi_0} (2\pi l)$. Therefore, in the interorbitaltriplet case, a zero-energy channel exists along the vortex which delocalizes the MFs on the sample surface and suppresses the zero-bias signal in STM.

In Fig. 2 we verify the analytic results using a 3D lattice model with periodic boundary conditions along the z direction. Figure 2(a) shows the spectrum of the vortex modes for intraorbital-singlet pairing where the vortex gap closes solely when $\phi_B = \pi$. In contrast, Fig. 2(b) shows that for

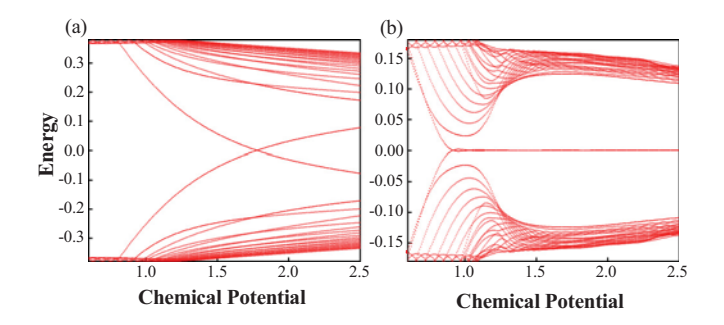


FIG. 2. Dependence of the vortex-mode energies on the chemical potential μ obtained from the 3D lattice model with periodic boundary conditions along the z direction for $k_z = 0$. (a) Intraorbital-singlet pairing $\Delta_1 = 0.4$ for $\Delta_Z = 0$. (b) Interorbital-triplet pairing $\Delta_0 = 0.4$ and $\Delta_Z = 0.2$. The parameters for the model are M = 4.5, $m_0 = -2.0$, and t = 1.0 with the calculation performed on a 48 × 48 lattice in the x-y plane. We observe a zero-energy mode state exists for all chemical potentials inside the conduction band when the pairing is interorbital-triplet type.

interorbital-triplet pairing, once the chemical potential is in the conduction band, the system develops vortex zero modes which remain gapless for all chemical potentials. Thus, increasing the Zeeman coupling results in a shift of the Fermi surfaces that destabilize the intraorbital-singlet pairing in favor of the interorbital-triplet pairing leading to the omnipresence of a zero mode in the vortex core.

In Fig. 3, we examine the manifestation of the change in superconducting pairing by inserting a vortex in the tight-binding lattice model. We set $\mu=1.1t$, where t is the hopping amplitude in the lattice model. For small Zeeman couping, the intraorbital-singlet channel is dominant and the MFs are localized at the ends of the vortex on the surface. As the Zeeman splitting is increased, we destabilize the intraorbital-singlet

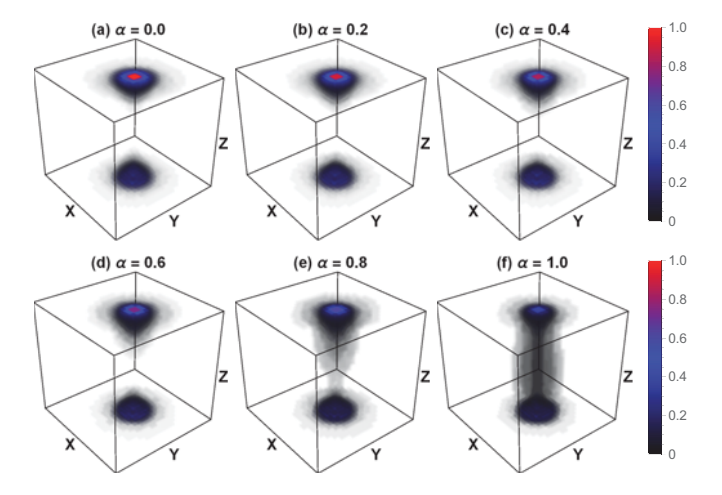


FIG. 3. Spatial profile of the lowest-energy vortex mode in 3D slab geometry for different values of parameter α , which controls the amplitude of the interorbital-triplet pairing $\Delta_0 = \alpha \Delta_0^0$, intraorbital s-wave $\Delta_1 = (1-\alpha)\Delta_1^0$, and Zeeman field $\Delta_Z = \alpha \Delta_Z^0$ around the vortex. The calculation is performed on a 24 × 24 × 24 lattice. The parameters used are $\mu = 1.1$, $\Delta_0^0 = 0.4$, $\Delta_1^0 = 0.4$, $\Delta_Z^0 = 0.2$, M = 4.5, $m_0 = -2.0$, and t = 1.0.

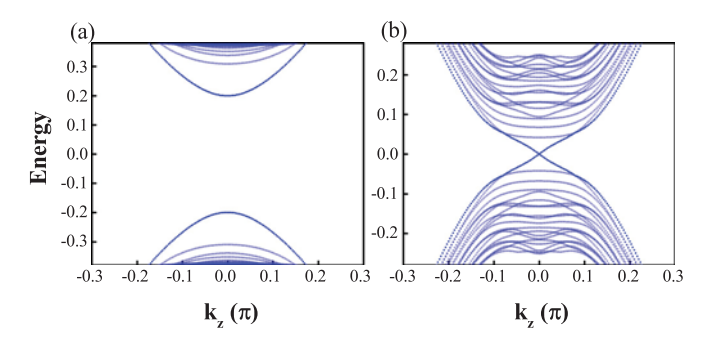


FIG. 4. k_z momentum dependence of the vortex modes for (a) intraorbital s-wave pairing $\Delta_1=0.4$ and (b) interorbital-triplet pairing $\Delta_0=0.4$ with $\Delta_Z=0.2$ and the chemical potential set to be $\mu=1.1$. Additional parameters of the model are the same as in Fig. 2.

pairing channel in favor of interorbital-triplet pairing allowing MFs to penetrate into the bulk. At sufficiently high Zeeman coupling, intraorbital-singlet pairing is fully suppressed and MFs on the surface delocalize through the vortex modes and extend into the bulk of the superconductor. As will be shown below, this mechanism would only delocalize the Majorana zero modes and not the finite-energy states.

Effective 1D vortex model. Using the vortex-mode wave functions $\Psi_V^{\nu}(l,r)$, we now derive an effective Hamiltonian for the modes along the vortex line connecting the sample surfaces [44]. To this end, we calculate the matrix elements of the k_z -dependent terms in the Hamiltonian (1), within the space of the two families of vortex modes $\Psi_V^{\nu}(l,r)$. Defining η_i as Pauli matrices acting on the space of the two sets of modes, the effective vortex Hamiltonians have the general form

$$H_V^l(k_z) = \frac{E_l^+ + E_l^-}{2} \eta_0 + \left(\frac{E_l^+ - E_l^-}{2} + \tilde{\epsilon}_l k_z^2\right) \eta_z - \tilde{v}_z k_z \eta_x.$$
(6)

Here, E_l^{ν} are the energies of the lth vortex modes coming from the Fermi surface corresponding to $\nu=\pm$ and increasing monotonically with l for fixed ν . $\tilde{\epsilon}_l$ and \tilde{v}_z are parameters of the k_z -dependent terms, projected into the lth vortex mode. Nambu particle-hole symmetry is given by $\mathcal{P}^{-1}[H_V^l(k_z)]\mathcal{P}=H_V^{-l}(-k_z)=-H_V^l(k_z)$, which implies $E_{-l}^{\pm}=-E_l^{\pm}$ and $\tilde{\epsilon}_l=-\tilde{\epsilon}_{-l}$ as shown in Ref. [30]. For each $l\neq 0$, Eq. (6) realizes a Z_2 topological state with modes with an angular momentum l localized at the ends of the vortex and finite energy if $(E_l^+-E_l^-)\tilde{\epsilon}_l<0$ [45]. Since the Zeeman field is along the flux line, we have $k_F^+< k_F^-$, which implies $\mathrm{sgn}(E_l^+-E_l^-)=\mathrm{sgn}(l)$ and reduces the above condition to $\epsilon<0$; this is true for FTS, whose normal state corresponds to a doped TI. The particle-hole partner of these states corresponds to angular momentum -l. The perturbations could modify the energy of these modes in pairs such that particle-hole symmetry is respected.

In contrast, Nambu particle-hole symmetry implies $E_0^{\pm} = 0$ as well as $\epsilon_0 = 0$, so the vortex is gapless when the pairing is of purely interorbital-triplet form. As shown in Fig. 4(b), the effective vortex Hamiltonian for the zero-energy states is linearly dispersing with momentum along the vortex. However, Nambu symmetry permits a mass term $\propto \eta_v$; indeed, remnant

singlet pairing outside of the vortex induces the scattering between vortex modes coming from different Fermi surfaces, producing a term $\eta_y \Delta_s^{Vrx}$ [30]. Δ_s^{Vrx} is k_z independent, thus making the vortex topologically *trivial* and devoid of zero modes at its ends.

We note that the energy levels at the vortex ends ε_l are equally spaced and are labeled by integers l, which corresponds to the angular momentum associated with the rotational symmetry of the vortex. The only patterns for such vortex-mode energies that are consistent with particle-hole symmetry are $\varepsilon_l \propto l$ and $\varepsilon_l \propto l+1/2$. The former contains a zero mode while the latter does not. Since, as argued above, the vortex is topologically trivial and lacks zero modes at its ends when the Zeeman-driven orbital-triplet pairing dominates, $\varepsilon_l \propto l+1/2$ in this case. On the other hand, if intraorbital-singlet pairing dominates, the vortex ends up being topological and its ends have a spectrum containing the zero modes [41] and satisfies $\varepsilon_l \propto l$. These results are in accordance with the two types of vortex spectra seen in Ref. [22].

A Zeeman coupling in the vortex regions can be mediated by the magnetic impurities present along the vortex. For such an effect to have a notable experimental signature, however, it is crucial for the vortices to be attracted to the magnetic atoms. A comparison of the energies of states where the vortices are far from the magnetic impurities with the case where the vortex is passing through the impurity is the direct method to examine the vortex impurity interactions. In addition to the surface tension of a vortex, the energy of the in-gap Shiba states at the magnetic impurity site [46-48] and the CDM modes define the energy cost of vortex creation. A recent study directly compared the energy of these in-gap states for the case where the vortex and impurity are at the same location with the energy for the isolated vortex and impurity [31]. This study, which was performed for strongly spin-orbit coupled materials and aimed to study the effect of magnetic impurities in FTS, showed that the sum of the energy of the CDM and Shiba modes decreases when the vortex passes through the impurity. This general reduction in energy resulting from placing a vortex on the impurity provides a strong suggestion for the attractive interaction between vortices and impurities. The result of this attraction motivates our considerations which, as seen, leads to a depiction of the FTS vortex phenomenology in accordance with experimental data, without the need to invoke MF hybridizations.

Conclusion. We have examined the effect of Zeeman coupling on the structure of vortex modes in FTS. We find that intraorbital-singlet pairing, which supports MFs at the ends of the vortices, is suppressed by the Zeeman field and is replaced with interorbital-triplet pairing, with only finite-energy vortex modes at the ends of the vortex.

The property of the FTS that facilitates our models is the degenerate Fermi surfaces that are split into two helical Fermi surfaces by the Zeeman field. The size of the superconducting gap in FTS is of the order of 2.5 meV for the hole pocket and 4.2 meV for the electron pocket [18,33,34], and the sizes of the Fe impurity dipole moments are of the order of 5 μ_B [31,33]. Given the average distance of the Fe impurity atoms, their associated Zeeman coupling is of the order of $\Delta_Z \approx 7.84$ meV. It is then evident that the Zeeman coupling can

affect the form of the superconducting pairing. We demonstrate that the nature of the vortices in FTS is inextricably linked to the effect of Zeeman coupling, which determines the form of superconducting pairing and indicates that suppression of Zeeman coupling, by the reduction of magnetic impurities, stabilizes the vortex MFs in FTS. The importance of our proposed mechanism can be checked by observation of the effect of the density of the magnetic impurities on the fraction of vortices with MF vortex modes.

Acknowledgments. This research was supported under National Science Foundation Grants No. EFRI-1542863 and No. DMR-1824265, and a PSC-CUNY Award, jointly funded by

The Professional Staff Congress and The City University of New York (P.G.). P.L.S.L. is supported by the Canada First Research Excellence Fund. A.G. is support by the European Union's Horizon 2020 research and innovation program under the Marie Skłodowska-Curie Grant Agreement No. 754411. P.H. was supported by the Department of Physics and the College of Natural Sciences and Mathematics at the University of Houston. M.J.G. acknowledges financial support from the National Science Foundation (NSF) under Grant No. DMR-1720633, CAREER Award No. ECCS-1351871, and the Office of Naval Research (ONR) under Grant No. N00014-17-1-3012.

- [1] Y. Li and Z.-A. Xu, Adv. Quantum Technol. 2, 1800112 (2019).
- [2] M. Sato and Y. Ando, Rep. Prog. Phys. 80, 076501 (2017).
- [3] L. Fu and C. L. Kane, Phys. Rev. Lett. 100, 096407 (2008).
- [4] R. M. Lutchyn, J. D. Sau, and S. Das Sarma, Phys. Rev. Lett. 105, 077001 (2010).
- [5] V. Mourik, K. Zuo, S. Frolov, S. Plissard, E. Bakkers, and L. Kouwenhoven, Science 336, 1003 (2012).
- [6] S. Nadj-Perge, I. K. Drozdov, J. Li, H. Chen, S. Jeon, J. Seo, A. H. MacDonald, B. A. Bernevig, and A. Yazdani, Science 346, 602 (2014).
- [7] N. Hao and J. Hu, Natl. Sci. Rev. 6, 213 (2018).
- [8] P. Dai, Rev. Mod. Phys. 87, 855 (2015).
- [9] R. P. Day, G. Levy, M. Michiardi, B. Zwartsenberg, M. Zonno, F. Ji, E. Razzoli, F. Boschini, S. Chi, R. Liang, P. K. Das, I. Vobornik, J. Fujii, W. N. Hardy, D. A. Bonn, I. S. Elfimov, and A. Damascelli, Phys. Rev. Lett. 121, 076401 (2018).
- [10] M. H. Christensen, J. Kang, and R. M. Fernandes, Phys. Rev. B 100, 014512 (2019).
- [11] V. Cvetkovic and O. Vafek, Phys. Rev. B 88, 134510 (2013).
- [12] A. Lau and C. Timm, Phys. Rev. B 90, 024517 (2014).
- [13] C. Youmans, A. Ghazaryan, M. Kargarian, and P. Ghaemi, Phys. Rev. B 98, 144517 (2018).
- [14] E. J. König and P. Coleman, Phys. Rev. Lett. 122, 207001 (2019).
- [15] R.-X. Zhang, W. S. Cole, X. Wu, and S. Das Sarma, Phys. Rev. Lett. 123, 167001 (2019).
- [16] T. Hanaguri, S. Niitaka, K. Kuroki, and H. Takag, Science 328, 474 (2010).
- [17] Z. Wang, P. Zhang, G. Xu, L. K. Zeng, H. Miao, X. Xu, T. Qian, H. Weng, P. Richard, A. V. Fedorov, H. Ding, X. Dai, and Z. Fang, Phys. Rev. B 92, 115119 (2015).
- [18] P. Zhang, K. Yaji, T. Hashimoto, Y. Ota, T. Kondo, K. Okazaki, Z. Wang, J. Wen, G. D. Gu, H. Ding, and S. Shin, Science 360, 182 (2018).
- [19] G. Xu, B. Lian, P. Tang, X.-L. Qi, and S.-C. Zhang, Phys. Rev. Lett. 117, 047001 (2016).
- [20] D. Wang, L. Kong, P. Fan, H. Chen, S. Zhu, W. Liu, L. Cao, Y. Sun, S. Du, J. Schneeloch, R. Zhong, G. Gu, L. Fu, H. Ding, and H.-J. Gao, Science 362, 333 (2018).
- [21] T. Machida, Y. Sun, S. Pyon, S. Takeda, Y. Kohsaka, T. Hanaguri, T. Sasagawa, and T. Tamegai, Nat. Mater. 18, 811 (2019).
- [22] L. Kong, S. Zhu, M. Papaj, H. Chen, L. Cao, H. Isobe, Y. Xing, W. Liu, D. Wang, P. Fan, Y. Sun, S. Du, J. Schneeloch, R.

- Zhong, G. Gu, L. Fu, H.-J. Gao, and H. Ding, Nat. Phys. 15, 1181 (2019).
- [23] S. Zhu, L. Kong, L. Cao, H. Chen, S. Du, Y. Xing, D. Wang, C. Shen, F. Yang, J. Schneeloch, R. Zhong, G. Gu, L. Fu, Y.-Y. Zhang, H. Ding, and H.-J. Gao, Science 367, 189 (2020).
- [24] C. Caroli, P. D. Gennes, and J. Matricon, Phys. Lett. 9, 307 (1964).
- [25] H. Lei, R. Hu, E. S. Choi, J. B. Warren, and C. Petrovic, Phys. Rev. B 81, 094518 (2010).
- [26] C.-K. Chiu, Y. H. T. Machida, T. Hanaguri, and F.-C. Zhang, arXiv:1904.13374.
- [27] S. Qin, L. Hu, X. Wu, X. Dai, C. Fang, F.-C. Zhang, and J. Hu, Sci. Bull. 64, 1207 (2019).
- [28] R.-X. Zhang, W. S. Cole, and S. Das Sarma, Phys. Rev. Lett. 122, 187001 (2019).
- [29] P. Zhang, Z. Wang, X. Wu, K. Yaji, Y. Ishida, Y. Kohama, G. Dai, Y. Sun, C. Bareille, K. Kuroda, T. Kondo, K. Okazaki, K. Kindo, X. Wang, C. Jin, J. Hu, R. Thomale, K. Sumida, S. Wu, K. Miyamoto, T. Okuda, H. Ding, G. D. Gu, T. Tamegai, T. Kawakami, M. Sato, and S. Shin, Nat. Phys. 15, 41 (2019).
- [30] See Supplemental Material at http://link.aps.org/supplemental/ 10.1103/PhysRevB.101.020504 for detailed calculations .
- [31] K. Jiang, X. Dai, and Z. Wang, Phys. Rev. X 9, 011033 (2019).
- [32] N. Zaki, G. Gu, A. M. Tsvelik, C. Wu, and P. D. Johnson, arXiv:1907.11602.
- [33] V. Thampy, J. Kang, J. A. Rodriguez-Rivera, W. Bao, A. T. Savici, J. Hu, T. J. Liu, B. Qian, D. Fobes, Z. Q. Mao, C. B. Fu, W. C. Chen, Q. Ye, R. W. Erwin, T. R. Gentile, Z. Tesanovic, and C. Broholm, Phys. Rev. Lett. 108, 107002 (2012).
- [34] J.-X. Yin, Z. Wu, J.-H. Wang, Z.-Y. Ye, J. Gong, X.-Y. Hou, L. Shan, A. Li, X.-J. Liang, X.-X. Wu, J. Li, C.-S. Ting, Z.-Q. Wang, J.-P. Hu, P.-H. Hor, H. Ding, and S. H. Pan, Nat. Phys. 11, 543 (2015).
- [35] P. Hosur, S. Ryu, and A. Vishwanath, Phys. Rev. B 81, 045120 (2010).
- [36] L. Fu and E. Berg, Phys. Rev. Lett. 105, 097001 (2010).
- [37] Y. Kim, T. M. Philip, M. J. Park, and M. J. Gilbert, Phys. Rev. B **94**, 235434 (2016).
- [38] S. Nakosai, Y. Tanaka, and N. Nagaosa, Phys. Rev. Lett. 108, 147003 (2012).
- [39] T. Hashimoto, S. Kobayashi, Y. Tanaka, and M. Sato, Phys. Rev. B 94, 014510 (2016).

- [40] P. Hosur, X. Dai, Z. Fang, and X.-L. Qi, Phys. Rev. B **90**, 045130 (2014).
- [41] P. Hosur, P. Ghaemi, R. S. K. Mong, and A. Vishwanath, Phys. Rev. Lett. **107**, 097001 (2011).
- [42] C.-K. Chiu, M. J. Gilbert, and T. L. Hughes, Phys. Rev. B **84**, 144507 (2011).
- [43] R. Jackiw and C. Rebbi, Phys. Rev. D 13, 3398 (1976).
- [44] P. L. e S. Lopes and P. Ghaemi, Phys. Rev. B 92, 064518 (2015).
- [45] X.-L. Qi and S.-C. Zhang, Rev. Mod. Phys. 83, 1057 (2011).
- [46] L. Yu, Acta Phys. Sin. 21, 75 (1965).
- [47] H. Shiba, Prog. Theor. Phys. 40, 435 (1968).
- [48] A. I. Rusinov, JETP Lett. 9, 85 (1969).